Faculty of Medicine
Biomedical Engineering

Master of Science Thesis

Title: Development of a Deep Learning-Based Model for the Detection of Extracapsular Extensions in Head and Neck

by

Léandre Cuenot

of (Heimatort or country of origin)

Supervisors
Prof. Dr. Mauricio Reyes and Dr. Daniel Schanne

Institutions
Institute for Surgical Technology & Biomechanics, Universität Bern
Universitätsklinik für Orthopedie und Traumatologie, Universität Bern

Examiners
Prof. Dr. Mauricio Reyes and Dr. Daniel Schanne

Bern, October 2024

Abstract

The abstract should provide a concise (300-400 word) summary of the motivation, methodology, main results and conclusions. For example:

Osteoporosis is a disease in which the density and quality of bone are reduced. As the bones become more porous and fragile, the risk of fracture is greatly increased. The loss of bone occurs progressively, often there are no symptoms until the first fracture occurs. Nowadays as many women are dying from osteoporosis as from breast cancer. Moreover it has been estimated that yearly costs arising from osteoporotic fractures alone in Europe worth 30 billion Euros.

Percutaneous vertebroplasty is the injection of bone cement into the vertebral body in order to relieve pain and stabilize fractured and/or osteoporotic vertebrae with immediate improvement of the symptoms. Treatment risks and complications include those related to needle placement, infection, bleeding and cement extravazation. The cement can leak into extraosseous tissues, including the epidural or paravertebral venous system eventually ending in pulmonary embolism and death.

The aim of this project was to develop a computational model to simulate the flow of two immiscible fluids through porous trabecular bone in order to predict the three-dimensional spreading patterns developing from the cement injection and minimize the risk of cement extravazation while maximizing the mechanical effect. The computational model estimates region specific porosity and anisotropic permeability from Hounsfield unit values obtained from patient-specific clinical computer tomography data sets. The creeping flow through the porous matrix is governed by a modified version of Darcy's Law, an empirical relation of the pressure gradient to the flow velocity with consideration of the complex rheological properties of bone cement.

To simulate the immiscible two phase fluid flow, i.e. the displacement of a biofluid by a biomaterial, a fluid interface tracking algorithm with mixed boundary representation has been developed. The nonlinear partial differential equation arising from the problem was numerically implemented into the open-source Finite Element framework *libMesh*. The algorithm design allows the incorporation of the developed methods into a larger simulation of vertebral bone augmentation for pre-surgical planning.

First simulation trials showed close agreement with the findings from relevant literature. The computational model demonstrated efficiency and numerical stability. The future model development may incorporate the morphology of the region specific trabecular bone structure improving the models' accuracy or the prediction of the orientation and alignment of fiber-reinforced bone cements in order to increase fracture-resistance.

Acknowledgements

Here you may include acknowledgements.

1. Please sign the following declaration if you did **not** use AI tools (like ChatGPT or DeepL)

„Ich erkläre hiermit, dass ich diese Arbeit selbstständig verfasst und keine anderen als die angegebenen Quellen benutzt habe. Alle Stellen, die wörtlich oder sinngemäss aus Quellen entnommen wurden, habe ich als solche gekennzeichnet. Ich erkläre weiter, dass ich keine unerlaubten Hilfsmittel verwendet habe, namentlich keine weiteren Personen mir beim Verfassen der Arbeit geholfen haben und ich keine Technologien der Künstlichen Intelligenz eingesetzt habe. Mir ist bekannt, dass andernfalls die Arbeit mit der Note 1 bewertet wird bzw. der Senat gemäss Artikel 36 Absatz 1 Buchstabe r des Gesetzes vom 5. September 1996 über die Universität zum Entzug des auf Grund dieser Arbeit verliehenen Titels berechtigt ist.
Für die Zwecke der Begutachtung und der Überprüfung der Einhaltung der Selbständigkeitserklärung bzw. der Reglemente betreffend Plagiate erteile ich der Universität Bern das Recht, die dazu erforderlichen Personendaten zu bearbeiten und Nutzungshandlungen vorzunehmen, insbesondere die schriftliche Arbeit zu vervielfältigen und dauerhaft in einer Datenbank zu speichern sowie diese zur Überprüfung von Arbeiten Dritter zu verwenden oder hierzu zur Verfügung zu stellen.“

1. Please sign the following declaration if you **did** use AI tools (like ChatGPT or DeepL). The use of AI tools must be permitted by your supervisor.

„Ich erkläre hiermit, dass ich diese Arbeit selbstständig verfasst und keine anderen als die angegebenen Quellen benutzt habe. Alle Stellen, die wörtlich oder sinngemäss aus Quellen entnommen wurden, habe ich als solche gekennzeichnet. Als Hilfsmittel habe ich Künstliche Intelligenz verwendet. Sämtliche Elemente, die ich von einer Künstlichen Intelligenz übernommen habe, werden als solche deklariert und es finden sich die genaue Bezeichnung der verwendeten Technologie sowie die Angabe der «Prompts», die ich dafür eingesetzt habe. Mir ist bekannt, dass andernfalls die Arbeit mit der Note 1 bewertet wird bzw. der Senat gemäss Artikel 36 Absatz 1 Buchstabe r des Gesetzes vom 5. September 1996 über die Universität zum Entzug des auf Grund dieser Arbeit verliehenen Titels berechtigt ist.
Für die Zwecke der Begutachtung und der Überprüfung der Einhaltung der Selbständigkeitserklärung bzw. der Reglemente betreffend Plagiate erteile ich der Universität Bern das Recht, die dazu erforderlichen Personendaten zu bearbeiten und Nutzungshandlungen vorzunehmen, insbesondere die schriftliche Arbeit zu vervielfältigen und dauerhaft in einer Datenbank zu speichern sowie diese zur Überprüfung von Arbeiten Dritter zu verwenden oder hierzu zur Verfügung zu stellen.“

Bern, October 27th 2024

Léandre Cuenot

Contents

Chapter 1

Introduction

Extracapsular extension (ECE) in head and neck cancers refers to the spread of metastatic tumors beyond the lymph node capsule into the surrounding connective tissue. ECE is associated with a poorer prognosis, significantly affecting treatment strategies and reducing overall survival rates in affected patients [4][7]. Accurate early detection of ECE is crucial for optimizing patient management and treatment planning. Proper identification of ECE can guide therapeutic decisions, including the potential benefits of adjunctive treatments such as postoperative concurrent chemoradiotherapy, which may improve outcomes for patients at higher risk due to ECE [6].

Currently, definitive diagnosis of ECE can only be confirmed through postoperative pathology, limiting its clinical utility [2]. In practice, contrast-enhanced computed tomography (CT) is used to detect ECE, relying heavily on physician expertise. Literature indicates that the sensitivity of CT for detecting ECE ranges from 18.8% to 72.2%, with higher sensitivity in more advanced cases. Sensitivity increases from 18.8% in early-stage (grade 1-2) ECE to 72.2% in advanced-stage (grade 4) ECE [8]. This wide range reflects considerable inter-observer variability.

Recent advancements in deep learning have shown significant potential in improving ECE detection compared to manual expertise [2][10][3]. Deep learning algorithms offer more consistent assessments and address the high inter-observer variability observed among human experts. Notably, the HECKTOR challenge, held annually from 2020 to 2022, focused on enhancing segmentation tasks through deep learning. The challenge aimed to develop models for segmenting the primary gross tumor volume (GTVp) and metastatic lymph nodes (GTVn) in the head and neck region. The results were promising, with a substantial majority of participants achieving an aggregate Dice similarity coefficient greater than 0.70 for both GTVp and GTVn, and the top-performing model achieving a Dice score of 0.788, underscoring the efficacy of deep learning approaches in complex segmentation tasks.

In this study, we propose an approach inspired by participants of the HECKTOR challenge, utilizing the same dataset, which integrates positron emission tomography (PET) imaging alongside conventional computed tomography (CT) imaging. PET imaging provides metabolic insights that complement the anatomical information from CT, potentially improving the detection of extracapsular extension (ECE) in head and neck cancers. By leveraging this multimodal approach, we aim to enhance diagnostic accuracy and provide more reliable predictions of ECE, thereby supporting more informed clinical decision-making.

The majority of the top-performing models in this domain have employed ensembles of 3D U-Net architectures. In this work, we aim to assess the robustness of 3D U-Nets under various perturbations that may occur in real-world clinical scenarios. Specifically, we will analyze how different tumor characteristics correlate with the degree to which these perturbations affect segmentation performance.

Additionally, we will link these findings to a relevant clinical application by comparing the model's performance with expert physicians' evaluations. This comparison will explore the correlation between the Dice similarity coefficient, which quantitatively assesses the segmentation accuracy of the deep learning models, and the qualitative assessment provided by physicians. Existing literature has demonstrated a moderate correlation between the Dice similarity coefficient and physician evaluations, with values ranging from 0.36 to 0.5 depending on the anatomical location of the segmented area [5].

Moreover, physicians will also evaluate cases with artificially introduced perturbations to examine whether changes in Dice scores align with variations in their clinical grading. This analysis will provide insights into the relationship between perturbation-induced segmentation errors and the clinical evaluation of ECE.

The primary focus of this study is on the segmentation aspect of the ECE prediction baseline. To enhance the overall predictive model, future work will extend the analysis to the classification component, aiming to improve the model's ability to predict ECE with greater accuracy.

Chapter 2

Methods

2.1 Hecktor dataset

For the segmentation model in this project, we utilized the dataset from the Hecktor Challenge 2022. This dataset consists of both training images with corresponding ground truth labels and test images without labels. For our purposes, we focused solely on the training subset due to the availability of ground truth annotations. This subset comprises 524 imaging cases collected from seven distinct clinical centers, including:

- CHUM: Centre Hospitalier de l'Université de Montréal, Montréal, Canada
- CHUP: Centre Hospitalier Universitaire de Poitiers, France
- CHUS: Centre Hospitalier Universitaire de Sherbrooke, Sherbrooke, Canada
- CHUV: Centre Hospitalier Universitaire Vaudois, Switzerland
- HGJ: Hôpital Général Juif, Montréal, Canada
- HMR: Hôpital Maisonneuve-Rosemont, Montréal, Canada
- MDA: MD Anderson Cancer Center, Houston, Texas, USA
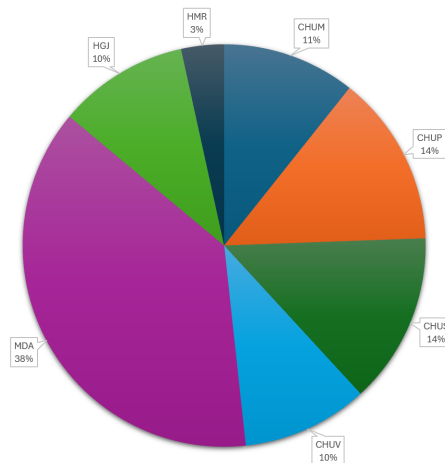
Figure 2.1. Distribution of cases across sites

Each case in the dataset contains two imaging modalities: computed tomography (CT), positron emission tomography (PET), and ground truth labels. The PET images were standardized using the Standardized Uptake Value (SUV). The CT and label images are provided in NIfTI format with a spatial resolution of 524×524 pixels in the axial plane, and variable depths across slices. While some CT images focus exclusively on the head and neck region, others encompass the entire body. In contrast, the PET images have a resolution of 128×128 pixels in the axial plane, with varying depths similar to the CT images.

(a) CT Scan (b) PET Scan (c) CT + PET and label
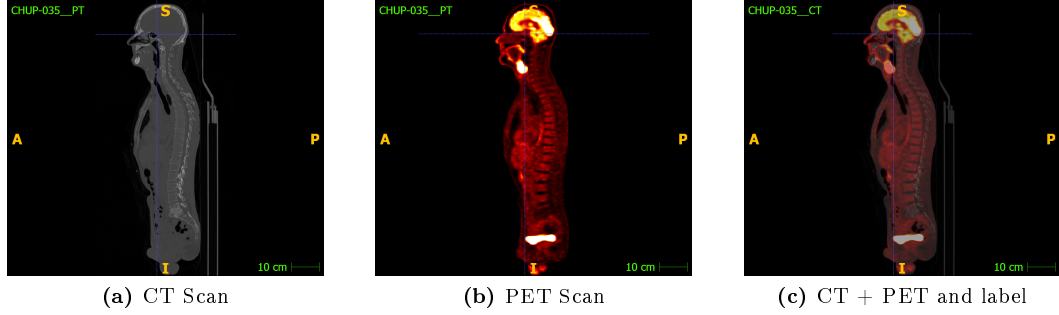
Figure 2.2. An example cases of the CHUP

2.2 Segmentation model

2.2.1 Preprocessing

Aspects of the preprocessing procedure were adapted from the methods employed by the winning team of the Hecktor Challenge 2022 [7] The initial preprocessing step involved resampling the PET images to achieve uniform dimensions across modalities. Specifically, PET images were resampled to an axial plane resolution of 524×524 pixels. Some labels exhibited minor dimensional discrepancies, occasionally differing by one plane in either width or height. These discrepancies were rectified following the resampling process.

Subsequently, after ensuring that all three imaging modalities (CT, PET, and label) were aligned to the same dimensions, the images were resampled to a common isotropic voxel size of 1×1×1 mm. This resampling was performed to facilitate subsequent cropping of the head and neck region.

For the cropping procedure, the center of the head was identified using the contours of the brain on the PET scan. Based on this central reference point, a subvolume of 200×200×[maximum of 310 pixels] was extracted. This approach minimizes the computational burden associated with background regions devoid of ground truth information. Additionally, the images underwent normalization via z-score clipping to mitigate the effects of outliers.

The processed images were saved in NIfTI format following the above steps. Further preprocessing techniques were applied during the training phase, which will be detailed in subsequent sections.

(a) CT Scan   **(b)** PET Scan   **(c)** CT + PET and label
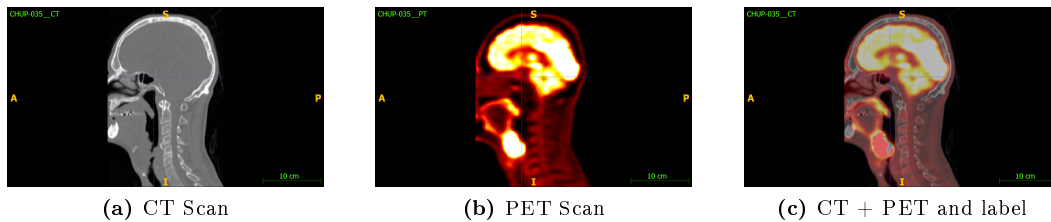
Figure 2.3. Same example cases after preprocessing

Chapter 3

A Sample Chapter

3.1 A Sample Section with a Table

3.1.1 Porosity Estimation

To parametrize the computational model the porosity of each foam type needs to be estimated from representative μCT data. Remember the definition of porosity as the ratio of the void volume and the total volume. μCT data is present in the form of binary data, i.e.

$$v_{m,n,p} \in \{0,1\} \qquad \forall m,n,p\,. \tag{3.1}$$

$v_{m,n,p}$ refers to the voxel value at instant position (m,n,p) in the three-dimensional μCT data array $\mathbf{V}$. Hence the porosity can be estimated as the ratio of voxels with an associated value of 0 and the overall number of voxels. Let

$$
\begin{aligned}
V &= \{v_{m,n,p}\} & \forall v_{m,n,p} &\in \mathbf{V} \\
V_0 &= \{v_{m,n,p}\} & \forall v_{m,n,p} &\in \mathbf{V} \wedge v_{m,n,p} = 0 \\
V_1 &= \{v_{m,n,p}\} & \forall v_{m,n,p} &\in \mathbf{V} \wedge v_{m,n,p} = 1 \\
& & V_0 \subseteq V\,, \quad V_1 &\subseteq V\,.
\end{aligned}
$$

V is the set of all voxels, V_0 the set of voxels with an associated value of 0 and V_1 the set of voxels with an associated value of 1 in the binary data array $\mathbf{V}$. Therefore $V = V_0 \cup V_1$. The porosity measure is then given by

$$\overline{\beta} = \frac{|V_0|}{|V|} = 1 - \frac{|V_1|}{|V|}\,. \tag{3.2}$$

$|S|$ is the *cardinality*, i.e. the size or number of members of the set S. Notice that $|V| = M \cdot N \cdot P$, meaning the size of the set V is equal to the number of voxels stored in the array $\mathbf{V}$.

The different porosity levels for the foams with $\{20, 30, 40\}$ PPI pore density are presented in Tab. 3.1.

Table 3.1. *All numbers are dimensionless* – Aluminum foam porosity levels estimated from representative μCT data.

	20 PPI	30 PPI	40 PPI
$|V|$:		78094368	
$|V_0|$:	73224007	68342720	59401544
$|V_1|$:	4870361	9751648	18692824
Porosity $\overline{\beta}$:	0.938	0.875	0.761

Chapter 4

Discussion and Conclusions

4.1 Discussion

Interpret your results in the context of past and current studies and literature on the same topic. Attempt to explain inconsistencies or contrasting opinion. Highlight the novelty of your work. Objectively discuss the limitations.

4.2 Conclusions

Formulate clear conclusions which are supported by your research results.

Chapter 5

Outlook

Provide a vision of possible future work to continue and extend your thesis research.

Bibliography

[1] V. Andrearczyk, V. Oreiller, and et al. Overview of the hecktor challenge at miccai 2022: Automatic head and neck tumor segmentation and outcome prediction in pet/ct. Lecture Notes in Computer Science, 13626(2):1–30, March 2023.

[2] B. H. Kann, S. Aneja, G. V. Loganadane, J. R. Kelly, S. M. Smith, R. H. Decker, J. B. Yu, H. S. Park, W. G. Yarbrough, A. Malhotra, B. A. Burtness, and Z. A. Husain. Pretreatment identification of head and neck cancer nodal metastasis and extranodal extension using deep learning neural networks. Scientific Reports, 8(5):14036, Sept. 2018.

[3] B. H. Kann and J. L. et al. Screening for extranodal extension in hpv-associated oropharyngeal carcinoma: evaluation of a ct-based deep learning algorithm in patient data from a multicentre, randomised de-escalation trial. Lancet Digital Health, 5(8):e360–e369, 2023.

[4] H. R. Kelly and H. D. Curtin. Squamous cell carcinoma of the head and neck: Imaging evaluation of regional lymph nodes and implications for management. Seminars in Ultrasound, CT, and MR, 38(1):466–478, Oct. 2017.

[5] F. Kofler, I. Ezhov, F. Isensee, and B. M. et al. Estimates of human expert perception for cnn training beyond rolling the dice coefficient. Melba, 2(9):27–71, May 2023.

[6] V. Krstevska. Evolution of treatment and high-risk features in resectable locally advanced head and neck squamous cell carcinoma with special reference to extracapsular extension of nodal disease. Journal of BUON, 20(6):943–953, July 2015.

[7] A. Myronenko, M. M. R. Siddiquee, D. Yang, Y. He, and D. Xu. Automated head and neck tumor segmentation from 3d pet/ct: Hecktor 2022 challenge report. In Proceedings of the HECKTOR 2022 Challenge, pages 31–37. Lecture Notes in Computer Science (LNCS, Volume 13626), 2023.

[8] R. S. Prabhu and K. R. M. et al. Accuracy of computed tomography for predicting pathologic nodal extracapsular extension in patients with head-and-neck cancer undergoing initial surgical resection. International Journal of Radiation Oncology Biology Physics, 88(3):122–129, Jan. 2014.

[9] T. V. Thomas, M. R. Kanakamedala, E. Bhanat, A. Abraham, E. Mundra, A. A. Albert, S. Giri, R. Bhandari, and S. Vijayakumar. Predictors of extracapsular extension in patients with squamous cell carcinoma of the head and neck and outcome analysis. Cureus, 13(4):e16680, July 2021.

[10] Y. S. e. a. Yoshiko Ariji. Ct evaluation of extranodal extension of cervical lymph node metastases in patients with oral squamous cell carcinoma using deep learning classification. Oral Radiology, 36(7):148–155, Apr. 2020.

Appendices

Appendix A

Vector and Tensor Mathematics

A.1 Introduction

...

A.2 Variable Types

...

Appendix B

Another Appendix

B.1 Section 1

...

B.2 Section 2

...